*Pramana – J. Phys.* (2017) 89:91
https://doi.org/10.1007/s12043-017-1490-0



# Rapid communication: $K^0_S$ Production from beryllium target using 120 GeV/c protons beam interactions at the MIPP experiment

A SINGH[1],*, A KUMAR[1], R RAJA[2], V BHATNAGAR[1] and V SINGH[3]

[1]Department of Physics, Panjab University, Chandigarh 160 014, India
[2]Fermi National Accelerator Laboratory, Batavia 50610, USA
[3]Banarus Hindu University, Varanasi 221 005, India
*Corresponding author. E-mail: amanphysics@gmail.com

MS received 13 April 2017; revised 5 September 2017; accepted 4 October 2017;
published online 30 November 2017

**Abstract.** We have measured the cross-section for the $K^0_S$ production from beryllium target using 120 GeV/c protons beam interactions at the main injector particle production (MIPP) experiment at Fermilab. The data were collected with target having a thickness of 0.94% of the nuclear interaction length. The $K^0_S$ inclusive differential cross-section in bins of momenta is presented covering momentum range from 0.4 GeV/c to 30 GeV/c. The measured inclusive $K^0_S$ production cross-section amounts to $39.54 \pm 1.46\delta_{\text{stat}} \pm 6.97\delta_{\text{syst}}$ mb and the value is compared with the prediction of FLUKA hadron production model.

**Keywords.** p + Be interactions; inclusive $K^0_S$ production cross-section.

**PACS Nos** **13.25.Es; 13.60.Hb; 13.75.Cs; 13.85.Ni**

## 1. Introduction

Fermilab main injector particle production (MIPP) spectrometer has been used to study the $K^0_S$ particle production during the interactions of 120 GeV/c protons beam with beryllium target. In the past, bubble chamber experiments have measured $K^0_S$ productions in hadron+proton interactions over a wide range of momentum [1–6] but the experimental data on $K^0_S$ productions from proton–nucleus interactions below and around 120 GeV/c are limited [7,8]. There are mainly two reasons to study the $K^0_S$ production at 120 GeV/c beam momentum. The first reason to study the $K^0_S$ meson production is for the precise neutrino flux measurement for the accelerator-based neutrino experiments at Fermilab. The $K^0_S$ production result will provide an important input for the precise calculation of the $\nu_e$ and $\bar{\nu}_e$ flux from $K^0_L \rightarrow \pi^{\mp} e^{\pm} \nu_e/\bar{\nu}_e$ decay. The second reason is that hadron–nucleus interactions will provide better understanding of strangeness and its interpretation as a signal of the onset of deconfinement in nucleus–nucleus interactions in this energy range because hadron–nucleus interactions is an intermediate step between hadron–hadron and nucleus–nucleus interactions. Therefore, this study will help one to understand the influence of nucleus matter on strangeness production.

The primary goal of the MIPP experiment was to measure the charged and neutral particle production cross-sections with high statistics and low systematical minimum-bias data and, also, to study the scaling laws in hadron fragmentation, to obtain the hadron production data for precise neutrinos flux measurement at NuMI target [9], to obtain inclusive neutron cross-section [10] and photon production data from hadron–nucleus interactions for proton radiography.

## 2. MIPP Spectrometer

The MIPP experiment (FNAL E907) [11] is a large acceptance spectrometer to measure the particle production on a variety of targets using protons, pions and kaon beams of both charges with momentum ranging from 5 to 120 GeV/c. It is located in Meson Centre at Fermilab. The systematic view of the MIPP spectrometer is shown in figure 1.

The spectrometer consists of two dipole magnets called 'Jolly Green Giant' and 'ROSSIE' magnets, for measuring charged particle momentum. The magnetic

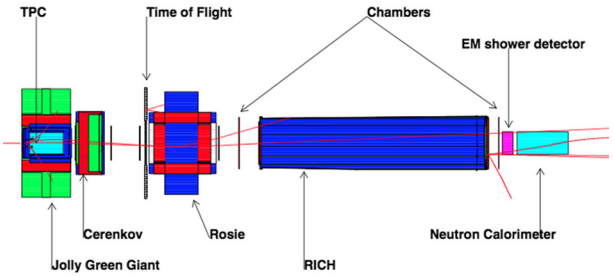


**Figure 1.** Schematic view of the MIPP spectrometer at Fermilab.

fields were set so that the kick angles were about equal and opposite. The track reconstruction of the incoming beam particles was done using three beam chambers (BC) located upstream of the interaction point. The trajectories of the outgoing charged particles were done using the hits from time projection chamber (TPC), four drift chambers (DC) and two multiwire proportional chambers (PWC). Primary and secondary vertices were found using the tracks that fall within some distance of the closest approach.

The charged particle identification at MIPP spectrometer was done using four subdetectors: time projection chamber (TPC), time of flight (TOF), Cherenkov detector (Chev) and ring imaging Cherenkov detector (RICH). TPC identified the charged particle in low momentum range (<1 GeV/c ) using means of ionization (d$E$/d$x$), TOF identified the particle in 1–3 GeV/c range, Cherenkov detector provided the PID in 3–17 GeV/c range and high momentum tracks (> 17 GeV/c) were identified using RICH detector. The neutral particles (i.e. gammas, neutrons) were identified in electromagnetic and hadron calorimeter.

The beryllium target was located 7 cm upstream of the entrance of the TPC and mounted on the target-wheel. The physical properties of the beryllium target are mentioned in ref. [10]. The scintillator counter having 7.6 cm × 0.32 cm × 5.1 cm dimension was placed immediately after the target. This counter worked as the interaction trigger. This interaction trigger has 100% efficiency for an event having more than three tracks.

## 3. Monte Carlo simulation

Monte Carlo simulation is used to correct the raw number of $K^0_S$ for detector effects (i.e. geometrical acceptance, reconstruction efficiency, interaction trigger efficiency etc.). Monte Carlo simulation of 120 GeV/c protons beam interactions with beryllium target was done using FLUKA2006 [12,13] for event generator and Geant3 [14] for particle tracking through MIPP spectrometer. FLUKA simulation produces primary, secondary etc. interactions of beam particles inside the target. The incoming beam momentum, spatial distributions, the outgoing charged particle momentum resolution and spatial resolution were simulated for TPC and wire chambers. Monte Carlo and data events were run through the same analysis and the same event selection cuts were applied. One of the main goal of this analysis is to compare the $K^0_S$ production cross-section with the prediction of FLUKA hadron production model.

## 4. Analysis technique

This section presents the event selection cuts for the beam flux measurement, track selection criteria to find the raw number of $K^0_S$ and corrections to the raw number of $K^0_S$. The analysis is based on $1.10 \times 10^6$ and $2.46 \times 10^5$ events collected using 120 GeV/c protons beam interactions with beryllium target inserted (target-in) and target removed (target-out) respectively.

### 4.1 *Event selection*

Event selection cuts were applied to reject events in which beam particles interacted with detector material instead of the target and to determine the incident beam flux. The incident beam flux was determined by counting the unbiased beam trigger events and then applied the run-dependent pre-scale factor that was set during the data taking. In this analysis, it is required to fire the interaction trigger to ensure an interaction in the target volume to produce ionization equivalent to 3 or more charged particles.

For overall event selection, we have applied the following conditions in the analysis:

1. Events with properly reconstructed single beam track, reconstructed using hits information recorded in three beam chamber located upstream of an interaction point, were retained so that initial state was well defined.
2. Events, whose reconstructed beam track time falls in 19 ns window from the accelerator RF bucket, were selected.
3. The reconstructed beam track transverse positions on upstream face of the target had to be consistent with the target's dimensions. The event having a beam radius less than 2 cm was selected, which ensures the interaction within the target volume. Figure 2 shows the radial position distribution of 120 GeV/c protons beam interactions with beryllium target.

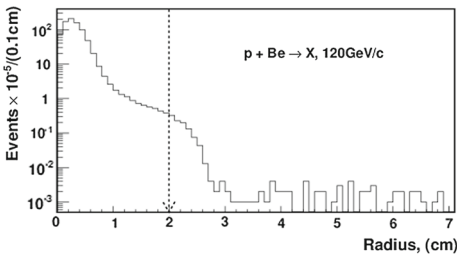


**Figure 2.** Radial positions of 120 GeV/c protons beam incident on beryllium target. The arrow indicates the location of the selection cuts.

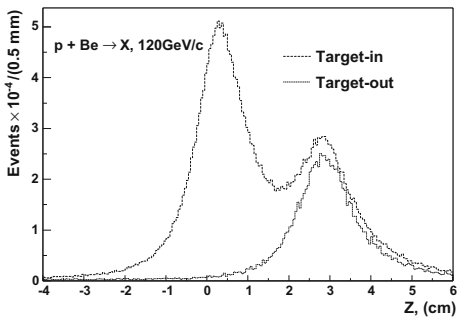


**Figure 3.** Primary $Z$ vertex distributions using 120 GeV/c protons beam interactions with beryllium target-in and target-out data.

4. Events from the target were required to have primary vertex not more than 4 cm upstream and 6 cm downstream of the target along the beam direction. The longitudinal primary vertice distribution using protons beam interactions with beryllium target (target-in) and target-out data are shown in figure 3. The interactions from the scintillator counter in target-in data was subtracted using the target-out data.
5. Number of tracks per event had to be more than three per event.

### 4.2 *Track selection cuts*

In this analysis, charged decay mode of $K^0_S$ is considered, which leads to two oppositely charged particles. In $K^0_S$ hypothesis, the positive (negative) charged particle assumed to be $\pi^+(\pi^-)$ meson and $K^0_S$ particles identified using an invariant mass of two opposite charged particles. Any pair of tracks, with opposite charge and distance of closest approach (DCA) between them smaller than 1 cm, is considered as a possible $V^0$ candidate. The following additional cuts were applied to select the $V^0$ candidates which correspond to $K^0_S$ with high probability:

1. The longitudinal distance along the beam direction between primary vertex and $V^0$ decay vertex had to be greater than 2 cm. This cut was used to reject cases in which primary tracks were wrongly reconstructed as $V^0$.
2. The impact parameter of the tracks from $V^0$ on the primary vertex had to be greater than 0.2 cm and impact parameter of $V^0$ line of flight on the primary vertex had to be less than 1.0 cm.
3. It is possible that $\Lambda(\bar{\Lambda})$ particles might be misidentified as $K^0_S$. Since proton is much heavier than pion, $\Lambda(\bar{\Lambda})$ decays are asymmetric in laboratory frame. Due to the isotropic decay of $K^0_S$ in its rest frame, a cut was applied on the angle between the $V^0$ line of flight and its positive charged particle in the centre of mass system. This cut was set as $-0.7 < \cos(\theta) < 0.7$ on $V^0$ combinations. Figure 4 shows the $\pi^+\pi^-$ vs. $p\pi^-$ invariant mass distributions before and after $\cos(\theta)$ track selection cut. It is clear from figure 4b that $\cos(\theta)$ cut removed the contamination of $\Lambda(\bar{\Lambda})$ particles from $K^0_S$ particles.
4. The $K^0_S$ decay time distribution decreases exponentially with time and the decay probability ($P_\mathrm{d}$) of a $K^0_S$ having momentum ($p$) with decay length ($d$) is given by

$$P_\mathrm{d} = 1 - \exp\left(\frac{-d}{\beta\gamma c\tau}\right). \quad (1)$$

Here $c\tau$ is 2.73 cm for $K^0_S$ and $\beta\gamma$ is the time dilation factor. A cut of $P_\mathrm{d} > 0.2$ was applied on all $V^0$ combinations.

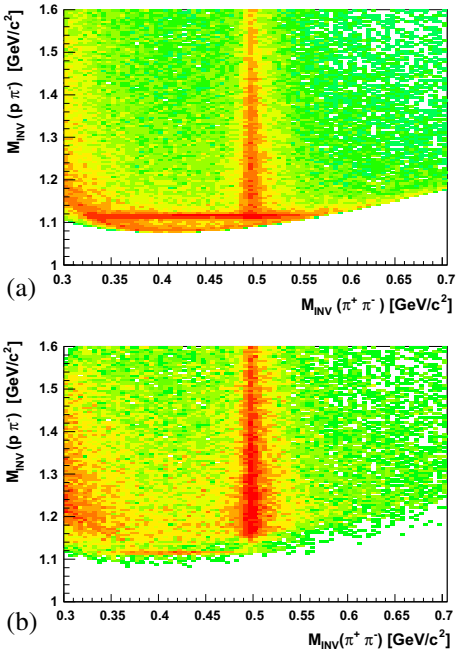


**Figure 4.** $\pi^+\pi^-$ and $p\pi^-$ distributions before and after $\cos(\theta)$ track selection cut. (**a**) Before $\cos(\theta)$ selection cut, (**b**) after $\cos(\theta)$ selection cut.

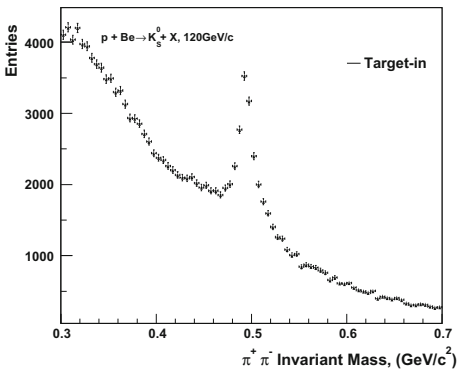


**Figure 5.** Hypothetical $\pi^+\pi^-$ invariant mass distribution using 120 GeV/c protons beam interactions with beryllium target.

All the above-mentioned cuts were applied on $V^0$ combinations and figure 5 shows the hypothetical $\pi^+\pi^-$ invariant mass distribution from beryllium target using 120 GeV/c protons beam interactions.

### 4.3 *Raw yields*

The hypothetical $\pi^+\pi^-$ invariant mass distributions were plotted in different momentum bins covering the range from 0.4 GeV/c to 30 GeV/c. The raw number of $K^0_S$ in each momentum bin was estimated using the fit function which was a sum of function $S(m)$ and fourth-order polynomial function for the signal and the background respectively. The $S(m)$ function is described as

$$S(m) = A\frac{\sigma/2}{(m-\mu)^2 + (\sigma/2)^2}, \tag{2}$$

where $A$ controls the height of the peak, $\sigma$ is the full-width at half-maximum (FWHM) and $\mu$ is the mean value of $K^0_S$ mass. The fit was performed in the invariant mass window (0.35–0.65) GeV/c$^2$. Figure 6 shows the invariant mass distributions of $\pi^+\pi^-$ in different bins of momenta from beryllium target using 120 GeV/c protons beam interactions. The integral of the $S(m)$ function estimated the raw number of $K^0_S$ in each momentum bin.

The raw number of $K^0_S$ from non-target interaction was subtracted using the information from events recorded with the target removed. The number of $K^0_S$ particles in a given momentum bin, corrected for non-target information, is estimated as

$$n = n_{\text{target-in}} \text{-} N n_{\text{target-out}}, \tag{3}$$

where $n_{\text{target-in}}$ and $n_{\text{target-out}}$ are the raw numbers of $K^0_S$ with target inserted and removed respectively. The factor $N$ can be determined from the beam fluxes from the target inserted and removed, using the following equation:

$$N = \frac{N^{\text{target-in}}_{B\text{flux}}}{N^{\text{target-out}}_{B\text{flux}}} \tag{4}$$

where $N^{\text{target-in}}_{B\text{flux}}$ and $N^{\text{target-out}}_{B\text{flux}}$ are the beam fluxes from the target inserted and the target removed respectively.

### 4.4 *Corrections*

The raw number of $K^0_S$ was estimated from the fit function and then corrections were applied to the raw number of $K^0_S$ to obtain the $K^0_S$ yield in the primary p–Be interactions. These corrections were obtained from Monte Carlo in which events were generated using FLUKA hadron production model and then these events were passed through full simulation of the MIPP detector. Following are the corrections which were applied to the raw number of $K^0_S$ particles.

1. Geometrical acceptance and reconstruction efficiency.
2. Correction due to the number of tracks greater than three per event cut.
3. Inefficiency of the interaction trigger.
4. Correction due to the primary longitudinal vertex cut.
5. Correction due to the track selection cuts.

The geometrical acceptance of $K^0_S$ was determined using the FLUKA model which included the size of the incident beam and its momentum distribution. For each generated $K^0_S$, we checked if charged particles ($\pi^+$and $\pi^-$) from the decay of $K^0_S$ projected inside the MIPP fiducial volume. Then for each momentum bin, the fraction of $K^0_S$ that fell into the MIPP fiducial volume gives the acceptance and found to be ≈99%. The charged particle reconstruction efficiency of MIPP is ≈90%. The $K^0_S$ reconstruction efficiency corresponds to reconstruction efficiency of the positive and negative charged particle tracks from $K^0_S$ decay. The $K^0_S$ reconstruction efficiency is found to be ≈70%. The reasons for low $K^0_S$ reconstruction efficiency as compared to charged particle reconstruction efficiency are due to two dead regions in the TPC chamber where charged particle somehow decay or stop and, in the other case, one charged particle from $K^0_S$ reconstructed but another opposite charged track could not be reconstructed due to low number of track's hits in the TPC chamber.

The correction factors for primary longitudinal vertex cut and number of tracks greater than three per event are less than 1%. The trigger inefficiency for $K^0_S$ analysis is less than 1% because the trigger efficiency is 100% for an event having more than three tracks. These corrections have negligible impact on $K^0_S$ analysis and are model-independent. The combined correction from

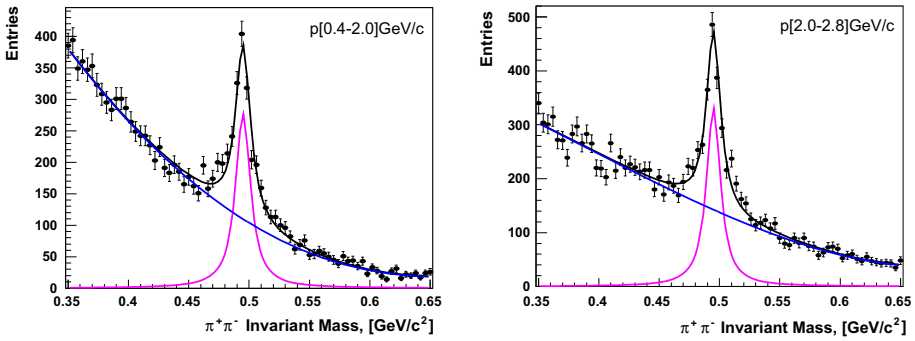


**Figure 6.** Hypothetical $\pi^+\pi^-$ invariant mass distributions in bins of momentum using 120 GeV/c protons beam interactions with beryllium target. Solid black line is the signal and background combined fit, solid blue line is the background fit and solid magenta line is the background-subtracted $\pi^+\pi^-$ invariant mass distribution.

Monte Carlo to the track selection cuts, mentioned in §4.2, is found to be ≈40% to $K^0_S$ particles.

## 5. $K^0_S$ Cross-section measurements

The $K^0_S$ inclusive differential cross-section in a bin of momentum is calculated as follows:

$$\frac{\mathrm{d}\sigma_{K^0_S}}{\mathrm{d}p} = \frac{N_{K^0_S}}{N_{\mathrm{beam}}} \times \frac{1}{n_t} \times \frac{1}{\Delta p} \times 10^4 \ (\mathrm{mb/GeV/c}). \quad (5)$$

Here $N_{K^0_S}$ is the corrected number of $K^0_S$ (corrected with branching ratio, geometrical acceptance, reconstruction efficiency, track selection cuts correction, trigger inefficiency and target-out subtraction), $N_{\mathrm{beam}}$ is the incident beam flux, $n_t$ is the number of nuclei per $\mathrm{cm}^2$ in the target, $\Delta p$ is the width of the momentum bin and factor $10^4$ is to bring the result to mb.

### 5.1 *Systematic errors*

Apart from the statistical error, systematic error on $K^0_S$ production cross-section is estimated. Following are the main sources of systematic errors:

1. The systematic uncertainty connected with the beam flux was studied. The beam flux ($N_{\mathrm{beam}}$) mentioned in §4.2 was compared with the beam flux determined using the counts from direct scalars accumulated during data taking. It was found that the relative difference between these two numbers was 8%. A conservative systematic uncertainty of 10% is assigned to the incident beam flux.
2. The systematic uncertainty due to primary longitudinal vertex cut was studied by varying this cut. In particular, the primary longitudinal vertex cut was varied to [−5.5, 7.5] cm and [−2.5, 4.5] cm from nominal value (i.e. [−4, 6] cm). The conservative 30% of the relative difference of $K^0_S$ production cross-sections due to modified primary longitudinal cut was assigned as systematic uncertainty on primary longitudinal vertex cut. The systematic uncertainty due to this cut was found to be less than 1%.
3. The systematic uncertainty due to track selection cuts was studied by varying all the cuts mentioned in §4.2. In particular, the distance of the closed approach cut was varied from 0.5 cm to 1.5 cm from the nominal value. The cuts 4.2(1), 4.2(2) and 4.2(4) were varied 0.5 and 1.5 times from the nominal values. The cut 4.2(3) was varied from [0.6, 0.6] to [0.8, 0.8]. The invariant mass window was changed to [0.4, 0.6] GeV/$\mathrm{c}^2$. The conservative 30% of the relative difference of $K^0_S$ production cross-sections due to the modified track selection cuts was assigned as systematic uncertainty. The overall systematic uncertainty due to track selection cuts was found to be less than 5%. A conservative 5% systematic uncertainty is assigned due to track selection cuts.
4. The systematic uncertainty connected with geometrical acceptances, reconstruction efficiency obtained from the Monte Carlo arises from MC statistics, imperfections in the geometry model of the spectrometer, imperfections in the modelling of the time-dependent performance of the tracking and incorrect modelling of the particle yields in the MC. The systematic error was estimated using the same procedure presented in [9]. The contributions of systematic uncertainties connected with geometrical acceptance and reconstruction efficiency are estimated to be 1% and 2% respectively.
5. The systematic uncertainty connected with the signal and background fitting functions was studied. The systematic uncertainty connected with signal fitting function was estimated by varying the signal function parameters with the corresponding uncertainties from the fit. For the background

fitting function, apart from the fourth-order polynomial function third-order polynomial function was used to estimate the systematic uncertainty due to background fitting function. The systematic uncertainty due to fitting function depends upon bin size and statistics. The total systematic uncertainty due to signal and background fitting functions is estimated to be ≈10%.

The systematic uncertainties due to sources discussed in points 1, 2 and 3 were found to be almost momentum-independent. The systematic uncertainties discussed in point 5 strongly depend on the selected momentum. The final systematic uncertainty in $K_S^0$ production cross-section was calculated as the sum in quadrature of error uncertainties discussed above. The combined systematic uncertainty is found to be ≈17% on $K_S^0$ production cross-section.

## 6. Results

Figure 7 shows the comparison of $K_S^0$ inclusive differential cross-section in bins of momenta with Monte Carlo predictions in 120 GeV/c protons beam interactions with beryllium target. The error bars on data points are the combined statistical and systematical errors. The $K_S^0$ production cross-section from beryllium target using 120 GeV/c protons beam interactions is $39.54 \pm 1.46\delta_{\text{stat}} \pm 6.97\delta_{\text{syst}}$ mb in comparison with 43.27 mb from FLUKA hadron production model. The combined statistical and systematic error on the data is ≈18%.

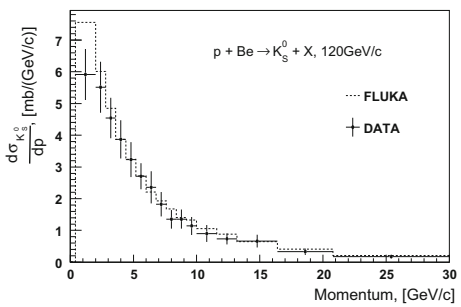


**Figure 7.** $K_S^0$ inclusive differential cross-sections from beryllium target using 120 GeV/c protons beam interactions in bins of momentum. Here error bars are combined statistical and systematical errors. Prediction of FLUKA hadron production model is superimposed.

## 7. Conclusion

We present the first measurements of the $K_S^0$ production cross-section from beryllium target using 120 GeV/c protons beam interactions at MIPP experiment at Fermilab. The inclusive differential production cross-section of $K_S^0$ was obtained in laboratory momentum bins covering the range from 0.4 GeV/c to 30 GeV/c and is compared with the prediction of FLUKA hadron production model. The FLUKA Monte Carlo gives $K_S^0$ production cross-section which is in reasonable agreement with our measurement within our overall uncertainty that is dominated by the systematic error.

## Acknowledgements

This work was supported by the US Department of Energy (DOE). The efforts of the Fermilab staff are gratefully acknowledged, whose successful efforts made this experiment possible.

## References

[1] H Blumenfeld *et al*, *Phys. Rev. Lett. B* **45**, 528 (1973)
[2] J M Champman *et al*, *Phys. Rev. Lett. B* **47**, 565 (1973)
[3] I V Ajinrnko *et al*, *Nucl. Phys. B* **165**, 1 (1980)
[4] J W Chapman *et al*, *Phys. Lett. B* **47**, 465 (1973)
[5] G Charlton *et al*, *Phys. Rev. Lett*. **30**, 574 (1973)
[6] F T Dao *et al*, *Phys. Rev. Lett.* **30**, 1151 (1973)
[7] P Zh Aslanyan *et al*, *Phys. Part. Nucl. Lett.* **4**, 60 (2007)
[8] M Yu Bogolyubsky *et al*, *Sov. J. Nucl. Phys.* **50**, 424 (1989)
[9] J M Paley *et al*, *Phys. Rev. D* **90**, 032001 (2014)
[10] T S Nigmanov *et al*, *Phys. Rev. D* **83**, 012002 (2011)
[11] R Raja, *Nucl. Instrum. Methods. Phys. Res. Sect. A* **553**, 225 (2005)
[12] A Fasso, A Ferrari, J Ranft and P R Sala, Reports No. CERN2005-10, No. INFN/TC05/11, and No. SLACR 773, (2005)
[13] A Fasso, A Ferrari, S Roesler, P R Sala, G Battistoni, F Cerutti, E Gadioli, M V Garzelli, F Ballarini, A Ottolenghi, A Empl and J Ranft, *Computing in High Energy and Nuclear Physics Conference* (2003), arXiv:physics/0306162
[14] R Brun *et al*, GEANT 3 Manual, CERN Program Library Long Writeup W5013, (1994)